Supporting Information

Sensing and Discrimination of Explosives at Variable Concentration with a Large-Pore MOF as part of a Luminescent Array

Monika Jurcic[†,∞], William J Peveler[‡,∞,*], Christopher N Savory[†], Dejan-Krešimir Bučar[†], Anthony J Kenyon[♦], David O Scanlon[†,▽] and Ivan P Parkin[†]

[†] Department of Chemistry, University College London, 20 Gordon Street, London, WC1H 0AJ, UK.
[‡] Division of Biomedical Engineering, School of Engineering, College of Science and Engineering, University of Glasgow, Glasgow G12 8LT, UK
[♦] Department of Electronic and Electrical Engineering, University College London, WC1E 7JE, UK.
[▽] Diamond Light Source Ltd., Diamond House, Harwell Science and Innovation Campus, Didcot, Oxfordshire OX11 0DE, UK

*william.peveler@glasgow.ac.uk

Additional Methods

Synthesis of **H_8L**:

The organic ligand 5,5',5",5"'-[1,2,4,5-benzenetetrayltetrakis(methylene-oxy)] tetra-1,3-benzenedicarboxylic acid (**H_8L**) was synthesised from a modified procedure[1]. Dimethyl 5-hydroxyisopthalate (6 mmol, 1.27 g) was dissolved in DMF (13 mL). A catalytic amount of KI (end of a spatula) was added to the solution whilst stirring, followed by K_2CO_3 (0.026 mol, 2.60 g). This solution was left to heat and stir at 100 °C for 1 hour. At this point 1,2,4,5-tetrakis(bromomethyl)-benzene (0.8 mmol, 0.288 g), dissolved in DMF (1 mL), was added to the mixture dropwise. The solution was further left for 1 hour at the same temperature with stirring. Subsequently the reaction was cooled to room temperature and 80 mL of H_2O was added to the reaction mixture to produce a white precipitate. The precipitate was filtered under vacuum and washed with portions of ice-cold water and dried under vacuum. This afforded the tetramethyl ester which was used without further processing.

The dry ester was added to a round bottom flask with 20 mL of MeOH, and an aqueous solution of NaOH (1.2 g in 12 mL) was added dropwise with stirring. This final solution was heated to 90°C and refluxed for 24 hours. After the solution was cooled to room temperature, it was then acidified to pH 1 with concentrated HCl and left to stir for an additional half an hour. The final precipitate was separated by filtration, washed with cold water and dried yielding H_8L as a white solid (544 mg 79.5% overall) ^{1}H NMR (DMSO-d6) δ 8.07 (4H, s), 7.82 (2H, s), 7.78 (8H, s), 5.42 (8H, s).

Sensing protocol

Solution-phase sensing experiments utilized stock solutions of MOF **MJ3'.** The suspensions were generated by adding 6 mg of finely ground active MOF **MJ 3'** to 6 mL of MeCN. These were ultrasonicated for three hours to generate the fine suspensions of the metal organic framework in solution.

Prior to the sensing of an explosive substance or related compound with **MJ3'**, 1.5 mL of a freshly ultrasonicated MOF **MJ3'** suspension sample was added to a quartz cuvette. The cuvette was then excited at 315 nm and emission measured between 330 - 600 nm. The fluorescence emission was re-measured on a 5 cycle time delay, recorded every 60 s, giving fluorescence emission spectra for t = 0, 60, 120, 180 and 240 s. Next, the sample was held on a vortexer, operating at 400 repetitions per minute for 15 s, and the fluorescence intensity was measured again. This was repeated 5 times in order to ensure a stable base line of the fluorescence emission intensity of the sample prior to analyte sensing.

For a sensing experiment, the MOF suspension was initially vortexed for 15 s to ensure the MOF particulates remained in suspension. After this, the initial fluorescence emission (I_0) of the suspension was measured, this was repeated twice more, with mixing between each reading, giving three baseline readings of the initial fluorescence emission of the MOF suspension prior to analyte addition. Explosive analytes were added in 10 µL aliquots, from 10 -100 µL, from the chosen stock solutions. Upon addition of a 10 µL explosive stock solution to the MOF suspension, the cuvette now containing the MOF and analyte, was vortexed for a further 15 s, and the fluorescence emission was measured (I). Two more 15 s vortex and fluorescence measurement cycles were undertaken, giving three fluorescence emission measurements for the addition of this volume of analyte to the solution. These steps were repeated for each further 10 µL addition of an explosive stock solution until 100 µL was added. Each sensing experiment was independently repeated, with fresh MOF suspensions, at least

three times. A 'blank' measurement was also performed with 10 µL additions of MeCN containing no explosive.

Each value of the triplicate values of I were averaged and used to calculate ($1- I/I_0$), a Quench Percentage (QP). This QP could then be further corrected by subtracting the quenching caused by MeCN dilution at that particular addition volume.

Optical characterisation of MOFs

UV-visible absorption spectra were measured on a Perkin Elmer Lambda 25 instrument, and excitation and emission spectra were measured on a Horiba Fluoromax 4 instrument, in 1 cm x 1 cm quartz cuvettes, at 1 nm resolution. Attempts to measure the quantum yield (QY) of **MJ3** in solution using both serial dilutions or an integrating sphere methodology were made, but no confident values could be obtained, due to the interference between the UV excitation wavelengths and the coating of the integrating sphere, and scattering/settling when using serial dilutions. Previous literature on MOF thin film QY measurements suggests values of between 1 and 30% are typical for MOFs composed of lanthanide emitters or closed shell d-metals, depending on their composition.

Single crystal X-ray diffraction measurements and analyses

Single X-ray diffraction data from a colourless and block-shaped crystal of **MJ3** (0.08 × 0.08 × 0.15 mm^3) was collected on a dual-source *Agilent SuperNova* single crystal X-ray diffractometer using a micro-focus Cu X-ray beam (λ=1.54184 Å, generated at 50 kV and 0.8 mA) and a 135 mm *Atlas* CCD detector. The sample temperature was controlled with an *Oxford Instruments Cryojet5*. The data was acquired, processed and corrected using the *CrysAlisPro* program.[1] Structure solution and refinement were accomplished using the *Olex2* program suite.[2] The structure was solved using a charge-flipping procedure,[3] while structure refinement was accomplished using *olex2.refine*, a refinement engine that is integrated within the *Olex2* program.[4]

All non-hydrogen atoms were refined anisotropically, while hydrogen atoms associated with carbon atoms were refined isotropically in geometrically constrained positions. Large areas of the MOF entailed a number of diffuse electron-density peaks that could not be modelled as solvent molecules that have been used in the MOF synthesis. A solvent-mask procedure was applied to determine the solvent accessible regions of the MOF and the bulk-solvent contribution to the calculated structure factors.[5] An electron count of 3939 electrons was found for a single void of 15019 $Å^3$ per unit cell. The calculation of the solvent-accessible region did not take into account the hydrogen atoms affiliated with the paddle-wheel water molecules (their position could not be determined). The final framework structure was refined using a solvent-corrected hkl-file. The crystallographic and refinement parameters for **MJ3** are given in **Table S1**.

Table S1: Crystallographic and refinement parameters for **MJ3**.

compound	**MJ3**
chemical formula	$C_{42}H_{22}O_{24}Zn_4$
M_r / g mol^{-1}	1172.21
crystal system	orthorhombic
space group	*Fmmm*
a / Å	25.0266(5)
b /Å	28.3181(7)
c / Å	30.3737(6)
α / °	90
β / °	90
γ / °	90
V / Å^3	21526.0(8)
Z	8
D_c / gcm^{-3}	0.7233*
F(000)	4688.0
μ(CuK_α) / mm^{-1}	1.347
T / K	150(1)
crystal size / mm	0.08 × 0.08 × 0.15
index range	−30 → 25 −32 → 34 −37 → 36
collected reflections	22105
unique reflections	5061
R_{int}	0.0241
reflections with $I > 2\sigma(I)$	4037
no. parameters	169
$R(F)$, $F > 2\sigma$(F)	0.0465
$wR(F^2)$, $F > 2\sigma$(F)	0.1479
$R(F)$, all data	0.0534
$wR(F^2)$, all data	0.1623
Δ_r (min., max.) e Å^{-3}	−0.338, 1.313
CCDC deposition number	1552177

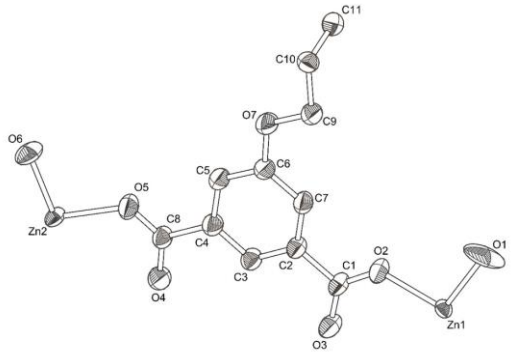

Figure S1: ASU for **MJ3** showing 2 Zn atoms and ¼ of linker **L**. Hydrogen atoms have been omitted for clarity and the thermal ellipsoids in the ASU are displayed at the 30% probability level.

Table S2: Comparison of MJ3 and Eddaoudi's MOF.

	MJ3	**Eddaoudi et al.[6]**
Formula	$Zn_4L(H_2O)_4$•(solvent)]$_n$	[$Cu_4L(H_2O)_4$•(solvent)]$_n$
a/Å	25.0266(5)	25.042(4)
b/Å	28.3181(7)	26.826(4)
c/Å	30.3737(6)	30.848(5)
α/°	90	90
β/°	90	90
γ/°	90	90
Volume/Å^3	21526.0(8)	20724(6)

Powder XRD of MJ3 and MJ3'

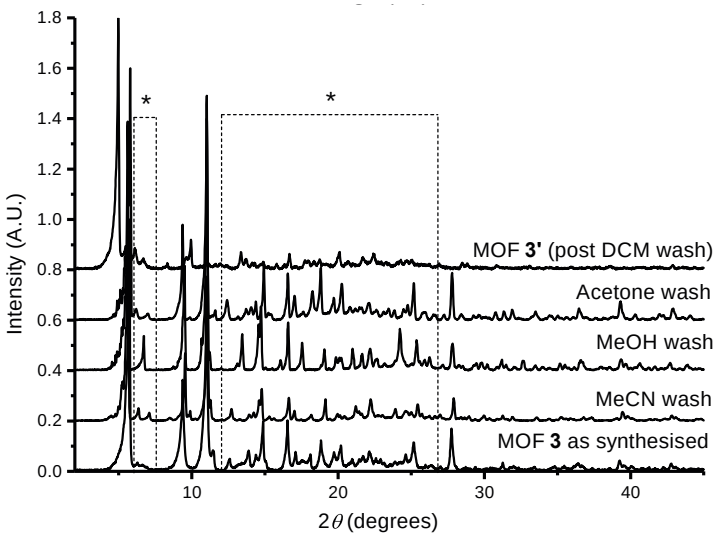

Figure S2: PXRD for MJ3 after each washing step, demonstrating long range order is maintained. Some small discrepancies in the peak positions, at short range, between each of the four washes were observed (marked with *), most noticeably for the activated material **MJ3'**, indicating some minor alterations in the MOF's structure upon solvent exchange and removal.

Computational Methods

For the MOF, calculations were performed using periodic DFT through the Vienna *Ab Initio* Simulation Package (VASP),[7,8,9,10] using the projector-augmented wave method was used to describe the core and valence electron interactions.[11] For geometry optimization, the PBEsol functional was used initially,[12] followed by PBE0[13] once the structure was close to convergence, which was determined once the forces on each atom were less than 0.01$Å^{-1}$. PBE0 was then used for all subsequent electronic calculations. The ionisation potential (IP) and electron affinity (EA) of the MOF were calculated using the method developed by Butler et al.[14] This method was previously used successfully for an alternate zinc-based fluorescent MOF.[15] A cut-off energy of 520 eV and, due to the large unit cell, Γ-point k-mesh sampling was used for all VASP calculations. In order to obtain accurate properties of the gas-phase analytes, they were calculated using DFT through the Gaussian09 package,[16] using Wilson et al.'s modification to the hybrid B97 functional (B972)[17] and Dunning's correlation consistent cc-pVTZ basis set, augmented with diffuse functions.[18] The IPs and EAs were calculated using the ΔSCF method, as described by Curtiss et al.[19], which has been used previously with hybrid DFT functionals to obtain values within 0.1 eV of experiment.[20]

Additional Figures for MJ3' sensing

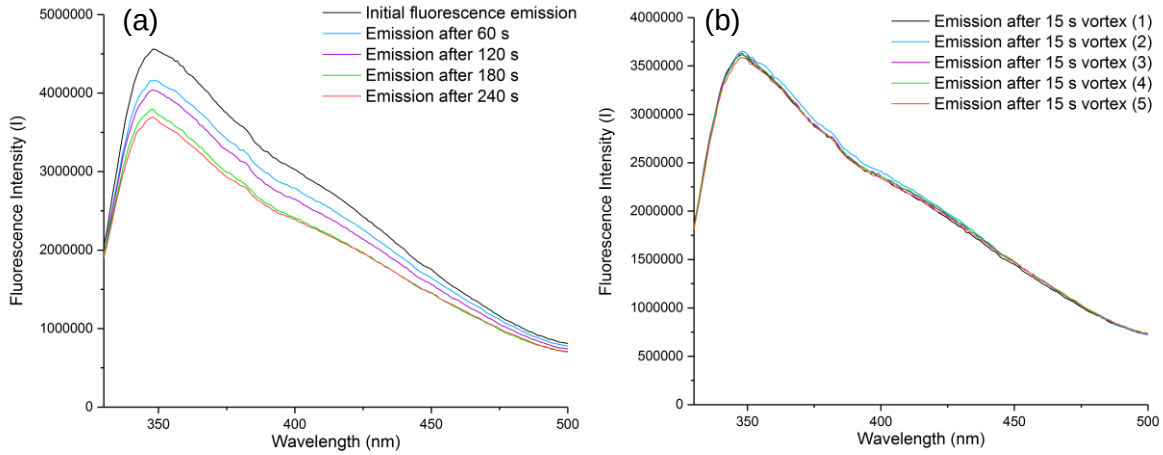

Figure S3: Stability of **MJ3'** suspensions in MeCN with (b) and without (a) vortexing.

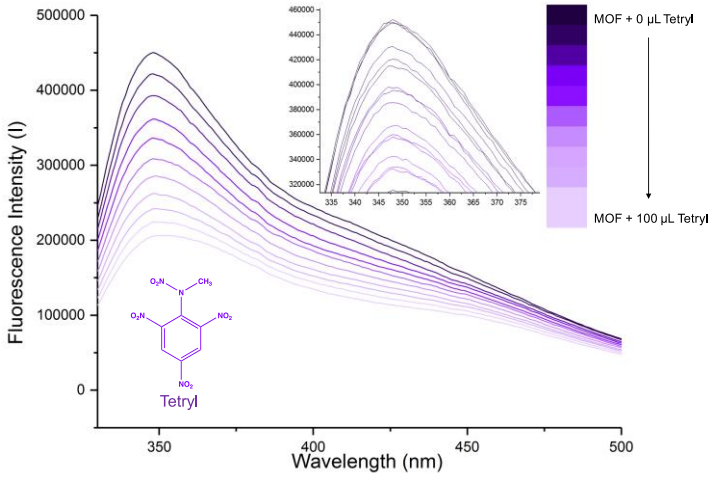

Figure S4: Quenching of **MJ3'** with Tetryl with inset showing small variations between repeats.

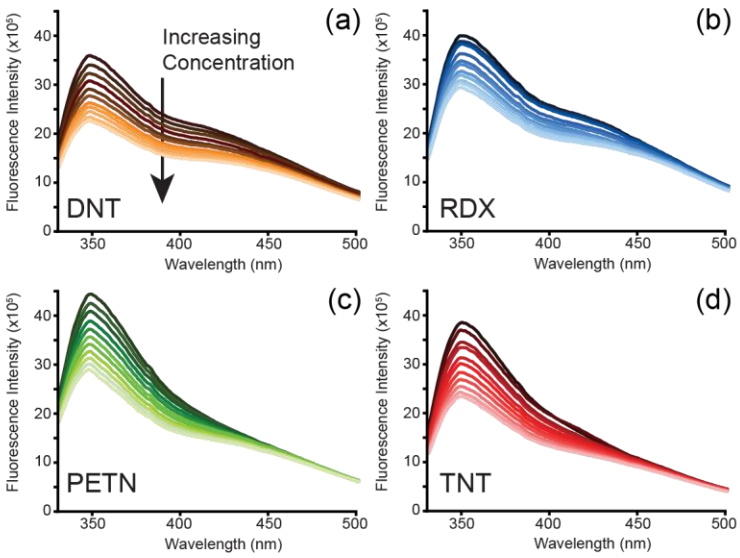

Figure S5: Quenching spectra for MJ3' solutions in MeCN with 100 µL additions of 1mM solutions of (a) DNT, (b) RDX, (c) PETN and (d) TNT.

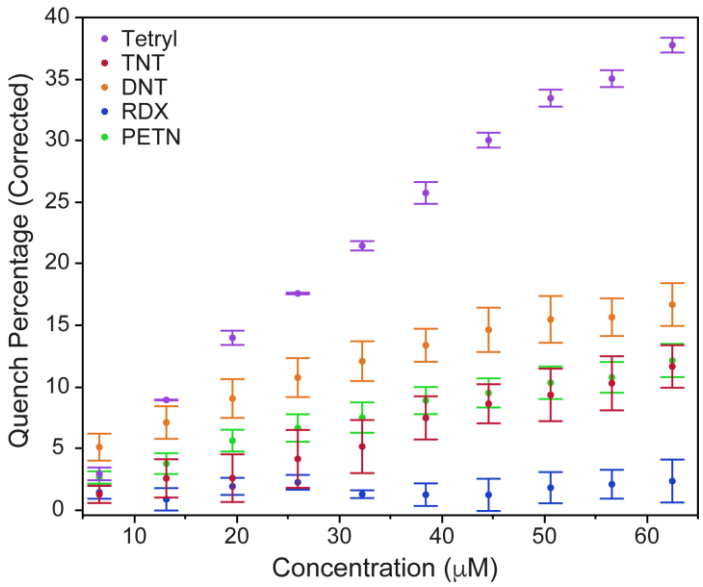

Figure S6: Corrected quenching percentages (Figure 3), accounting for dilution.

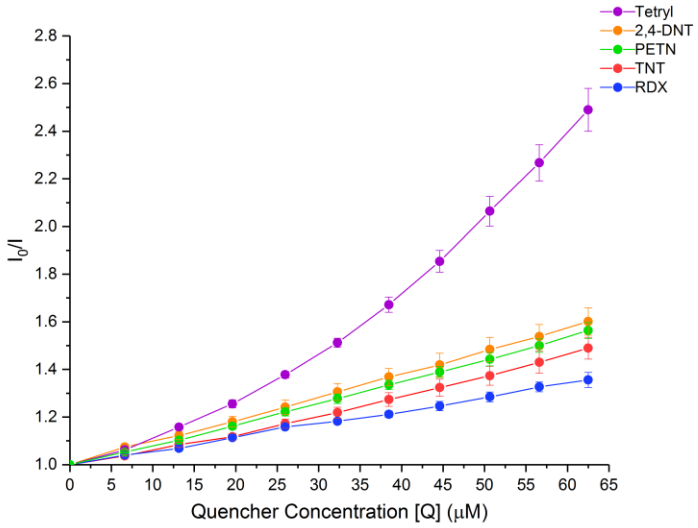

Figure S7: Quenching plots for each analyte with **MJ3'**. Error bars are one standard error on the mean. For the non-linear Tetryl, the first 4 points were used to measure a straight line.

Table S3: Quenching constants for each explosive. For Tetryl the first 4 points of the plot were fitted to ensure linearity.

Explosive	K_Q / M^{-1}	R^2
RDX	5.7 x 10^3	0.998
TNT	7.9 x 10^3	0.997
PETN	9.0 x 10^3	0.999
2,4-DNT	9.5 x 10^3	0.999
Tetryl	1.6 x 10^4	0.996

Table S4: Limits of Detection based on the methodology of Armbruster et al.[21]

Explosive	LOD / µM
2,4-DNT	3.19
Tetryl	3.98
TNT	5.32
RDX	5.32
PETN	5.76

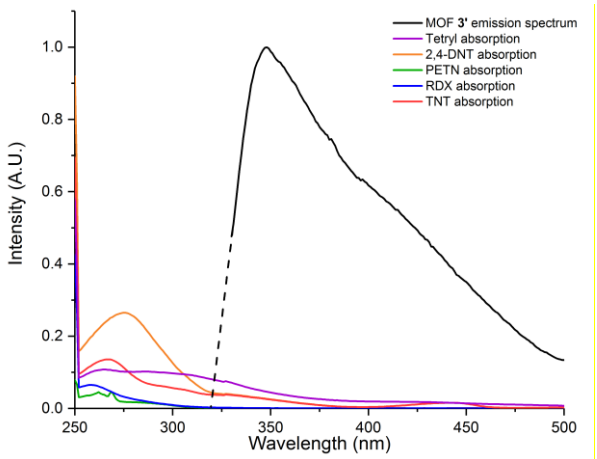

Figure S8: Potential optical overlap between MJ3 emission and absorption spectra of explosive stock solutions, showing largest overlap with Tetryl.

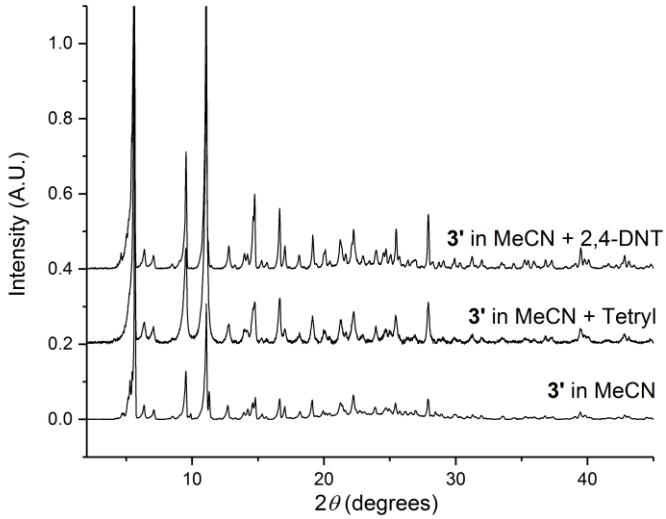

Figure S9: XRD of **MJ3'** before and after quenching with DNT or Tetryl showing very little change in powder XRD patterns.

Synthesis and Characterisation of Array MOFs

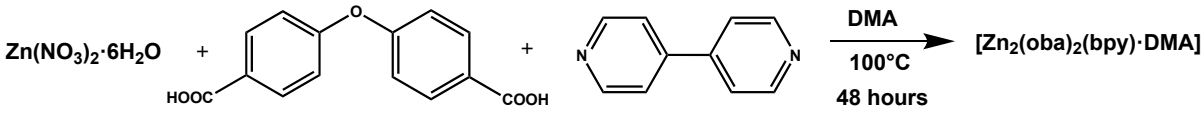

Figure S10: Synthesis scheme for **AM2** from Pramanik *et al.*[22]

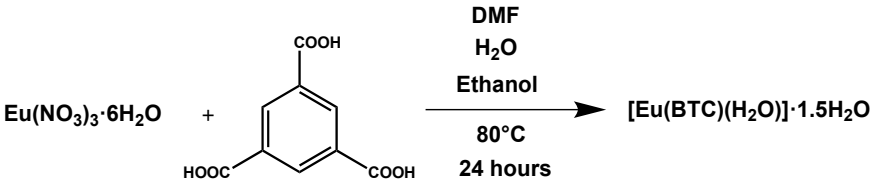

Figure S11: Synthesis scheme for **AM3** from Chen *et al.*[23]

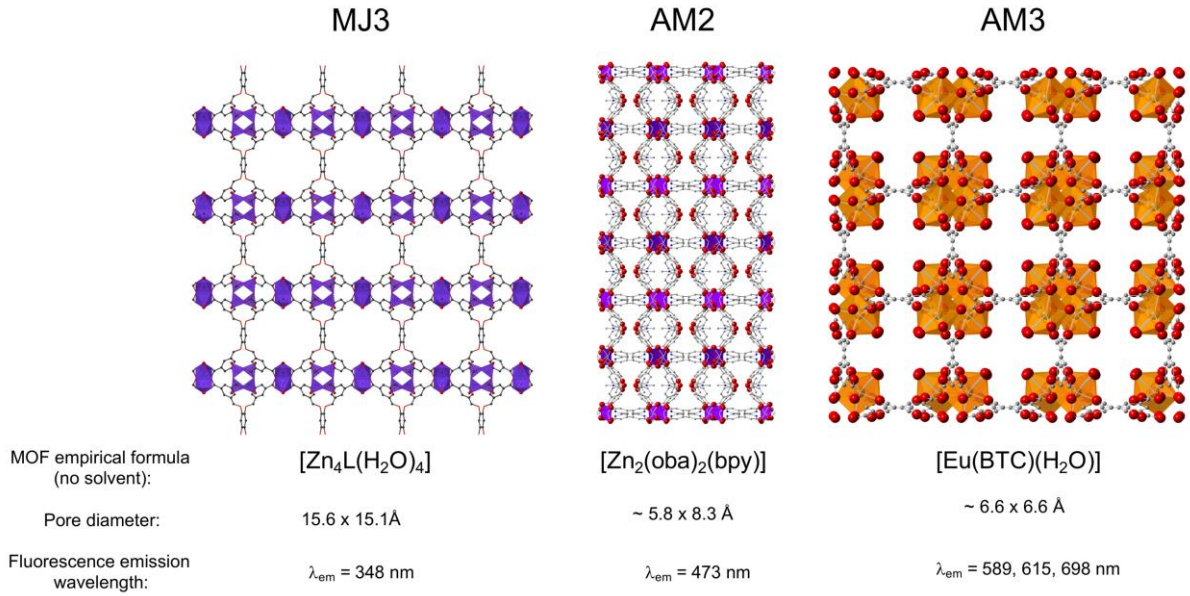

Figure S12: Comparative crystal structures and properties of **MJ3**, **AM2** and **AM3**. Adapted from references by Pramanik *et al.* and Chen *et al.*[19,20]

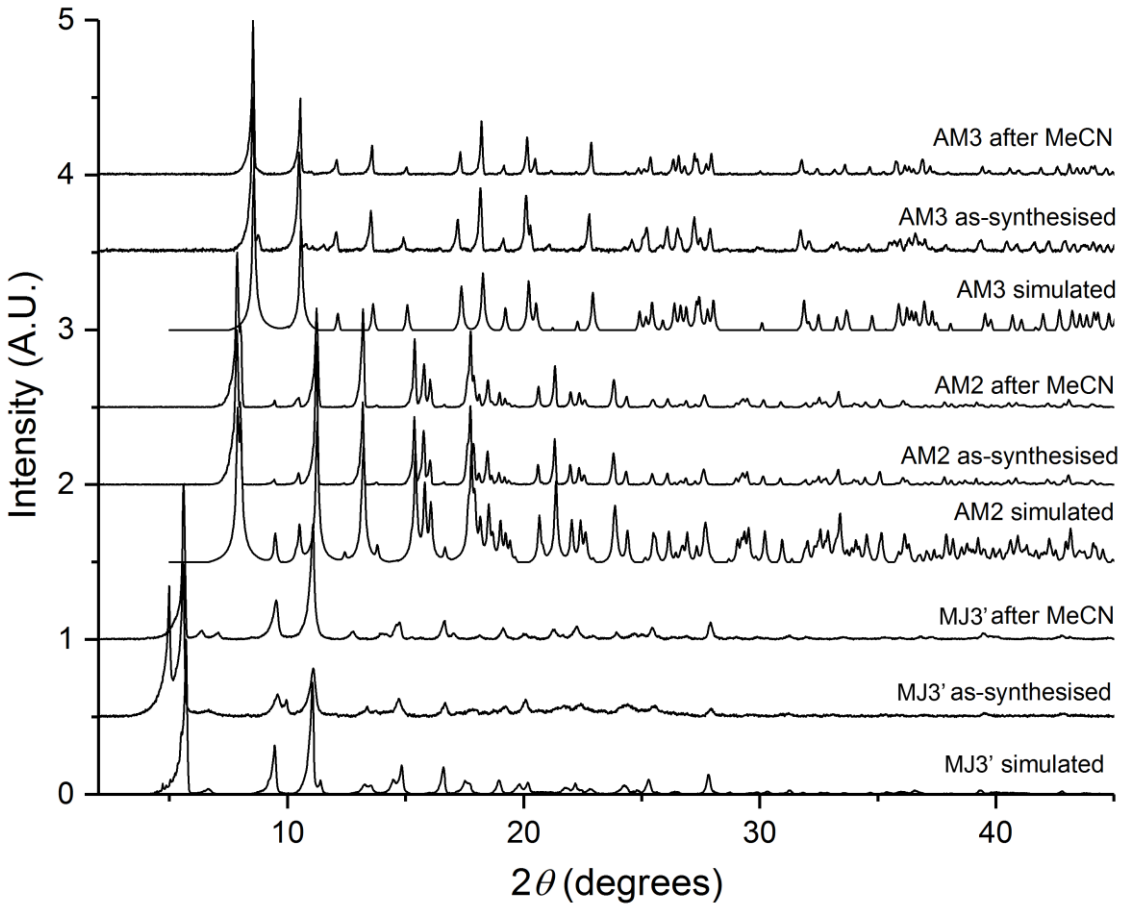

Figure S13: Powder XRD confirming the structure of the array MOFs **MJ3'**, **AM2** and **AM3**

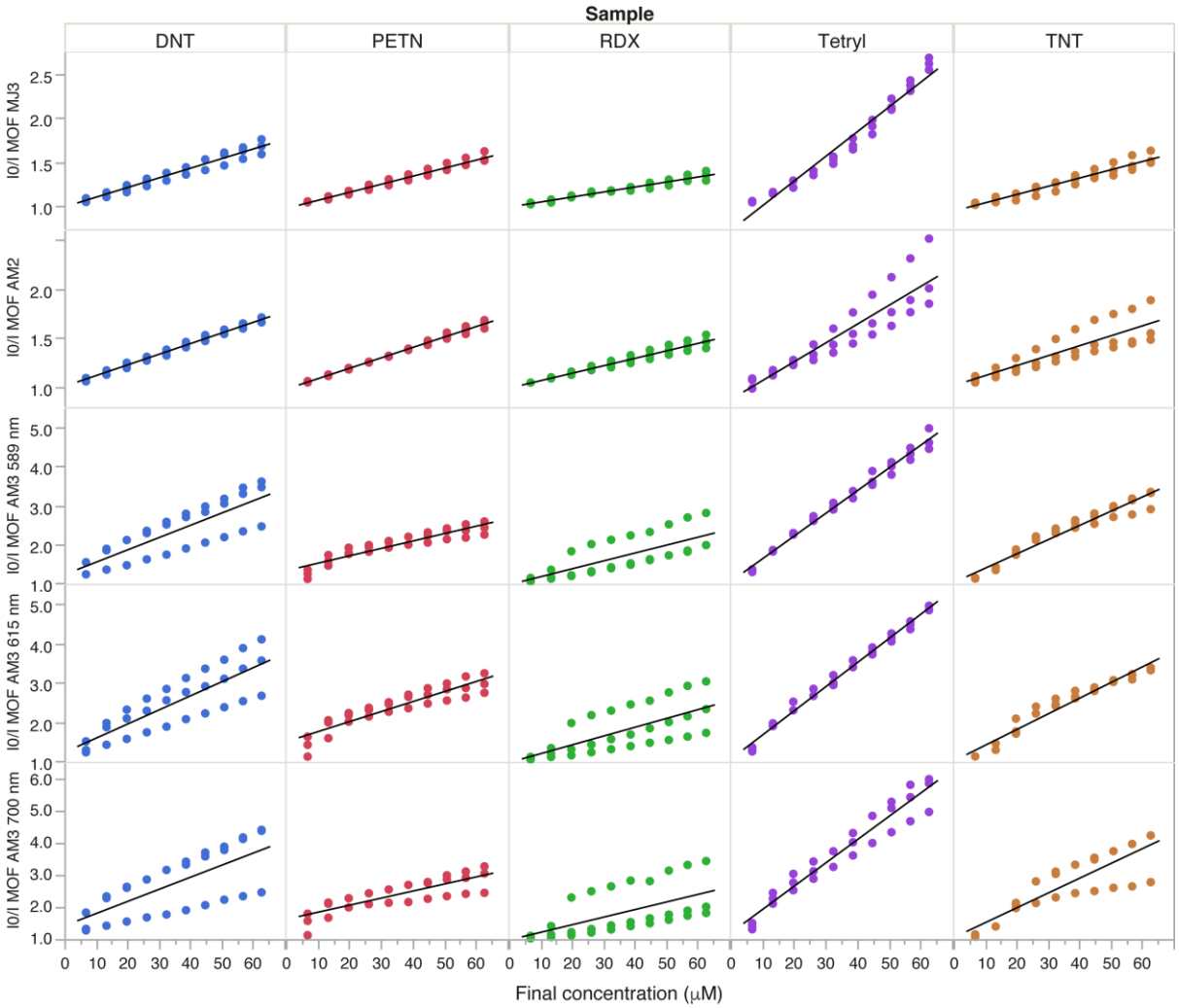

Figure S14: Individual array element responses. AM3 provides three responses across its three main emissive peaks at 589, 615 and 700 nm.

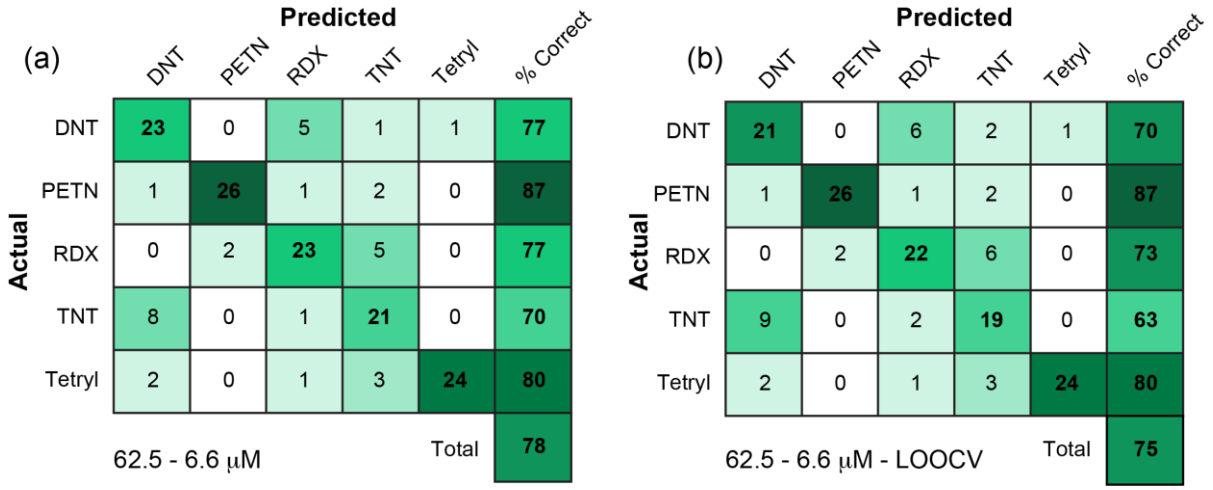

Figure S15: Confusion matrix for 6.6 - 62.5 μM explosives for (a) the LDA model, and (b) the Leave-one-out Cross Validation (LOOCV). PETN was remarkably well classified, even across this broad concentration range, however overall accuracy was lowered by TNT/DNT and TNT/RDX confusion.

References

[1] CrysAlisPro, Agilent Technologies, Version 1.171.37.34 (release 22-05-2014 CrysAlis171 .NET).
[2] Dolomanov, O. V.; Bourhis, L. J.; Gildea, R. J.; Howard, J. A. K.; Puschmann, H.; IUCr. OLEX2: a Complete Structure Solution, Refinement and Analysis Program. *J Appl Crystallogr* **2009**, *42* (2), 339–341.
[3] Oszlányi, G.; Sütő, A. The Charge Flipping Algorithm. *Acta Crystallogr., Sect. A.* **2008**, *64* (1), 123–134.
[4] Bourhis, L. J.; Dolomanov, O. V.; Gildea, R. J.; Howard, J. A. K.; Puschmann, H. The Anatomy of a Comprehensive Constrained, Restrained Refinement Program for the Modern Computing Environment – Olex2 Dissected. *Acta Crystallogr., Sect. A* **2015**, *71* (1), 59–75.
[5] Rees, B.; Jenner, L.; Yusupov, M. Bulk-Solvent Correction in Large Macromolecular Structures. *Acta Crystallogr D* **2005**, *61* (9), 1299–1301.
[6] Eubank, J. F.; Mouttaki, H.; Cairns, A. J.; Belmabkhout, Y.; Wojtas, L.; Luebke, R.; Alkordi, M.; Eddaoudi, M. The Quest for Modular Nanocages: Tbo-MOF as an Archetype for Mutual Substitution, Functionalization, and Expansion of Quadrangular Pillar Building Blocks. *J. Am. Chem. Soc.* **2011**, *133* (36), 14204–14207.
[7] Kresse, G.; Hafner, J. Ab Initiomolecular Dynamics for Liquid Metals. *Phys. Rev. B* **1993**, *47* (1), 558–561.
[8] Kresse, G.; Hafner, J. Ab Initiomolecular-Dynamics Simulation of the Liquid-Metal–Amorphous-Semiconductor Transition in Germanium. *Phys. Rev. B* **1994**, *49* (20), 14251–14269.
[9] Kresse, G.; Furthmüller, J. Efficiency of Ab-Initio Total Energy Calculations for Metals and Semiconductors Using a Plane-Wave Basis Set. *Comput. Mater. Sci.* **1996**, *6* (1), 15–50.
[10] Kresse, G.; Furthmüller, J. Efficient Iterative Schemes for Ab Initio Total-Energy Calculations Using a Plane-Wave Basis Set. *Phys. Rev. B* **1996**, *54* (16), 11169–11186.
[11] Blöchl, P. E. Projector Augmented-Wave Method. *Phys. Rev. B* **1994**, *50* (24), 17953–17979.
[12] Perdew, J. P.; Ruzsinszky, A.; Csonka, G. I.; Vydrov, O. A.; Scuseria, G. E.; Constantin, L. A.; Zhou, X.; Burke, K. Restoring the Density-Gradient Expansion for Exchange in Solids and Surfaces. *Phys. Rev. Lett.* **2008**, *100* (13), 136406.
[13] Adamo, C.; Barone, V. Toward Reliable Density Functional Methods Without Adjustable Parameters: the PBE0 Model. *J. Chem. Phys.* **1999**, *110* (13), 6158–6170.
[14] Butler, K. T.; Hendon, C. H.; Walsh, A. Electronic Chemical Potentials of Porous Metal-Organic Frameworks. *J. Am. Chem. Soc.* **2014**, *136* (7), 2703–2706.
[15] Jurcic, M.; Peveler, W. J.; Savory, C. N.; Scanlon, D. O.; Kenyon, A. J.; Parkin, I. P. The Vapour Phase Detection of Explosive Markers and Derivatives Using Two Fluorescent Metal–Organic Frameworks. *J. Mater. Chem. A* **2015**, *3* (12), 6351–6359.
[16] Frisch, M. J.; Trucks, G. W.; Schlegel, H. B.; Scuseria, G. E. *Gaussian 09, Revision A. 02. Gaussian Inc., Wallingford, CT*; 2009.
[17] Wilson, P. J.; Bradley, T. J.; Tozer, D. J. Hybrid Exchange-Correlation Functional Determined From Thermochemical Data and Ab Initiopotentials. *J. Chem. Phys.* **2001**, *115* (20), 9233–9242.
[18] Dunning, T. H., Jr. Gaussian Basis Sets for Use in Correlated Molecular Calculations. I. the Atoms Boron Through Neon and Hydrogen. *J. Chem. Phys.* **1989**, *90* (2), 1007–1023.
[19] Curtiss, L. A.; Redfern, P. C.; Raghavachari, K.; Pople, J. A. Assessment of Gaussian-2 and Density Functional Theories for the Computation of Ionization Potentials and Electron Affinities. *J. Chem. Phys.* **1998**, *109* (1), 42–55.
[20] Staroverov, V. N.; Scuseria, G. E.; Tao, J. M.; Perdew, J. P. Comparative Assessment of a New Nonempirical Density Functional: Molecules and Hydrogen-Bonded Complexes. *Journal of Chemical Physics* **2003**, *119* (23), 12129–12137.
[21] Armbruster, D. A.; Pry, T. Limit of Blank, Limit of Detection and Limit of Quantitation. *Clin Biochem Rev* **2008**, *29 Suppl 1*, S49–S52.
[22] Pramanik, S.; Zheng, C.; Zhang, X.; Emge, T. J.; Li, J. New Microporous Metal−Organic Framework Demonstrating Unique Selectivity for Detection of High Explosives and Aromatic Compounds. *J. Am. Chem. Soc.* **2011**, *133* (12), 4153–4155.
[23] Chen, B.; Yang, Y.; Zapata, F.; Lin, G.; Qian, G.; Lobkovsky, E. B. Luminescent Open Metal Sites Within a Metal–Organic Framework for Sensing Small Molecules. *Adv. Mater.* **2007**, *19* (13), 1693–1696.